Mechanically Stiffened and Thermally Softened Raman Modes of ZnO Crystal

J. W. Li, L. W. Yang,* Z. F. Zhou, X. J. Liu, G. F. Xie, and Y. Pan

Institute for Quantum Engineering and Micro-Nano Energy Technology, Key Laboratory of Low-Dimensional Materials and Application Technologies, and Faculty of Materials and Optoelectronic Physics, Xiangtan University, Hunan 411105, China

C. Q. Sun*,†

School of Electrical and Electronic Engineering, Nanyang Technological University, Singapore 639798, Singapore

Received: October 16, 2009; Revised Manuscript Received: December 16, 2009

An analytical form connecting the energy shift of Raman modes directly to the bonding identities (order, nature, length, energy) of a specimen and the response of the bonding identities to the applied stimuli of temperature and pressure was presented for a deeper understanding of the atomistic origin of the ZnO Raman shift. Theoretical reproduction based on the BOLS correlation theory [Sun, C. Q. *Prog. Solid State Chem.* **2007**, *35*, 1] and the local bond average (LBA) approach [Sun, C. Q. *Prog. Mater. Sci.* **2009**, *54*, 179] of the measurements revealed that the thermally softened ZnO Raman modes arise from bond expansion and bond weakening due to vibration and that the pressure-stiffened Raman modes result from bond compression and bond strengthening due to mechanical work hardening. The developed approach could be useful in generalizing the lattice dynamics directly to the process of vibration and relaxation of a representative bond of the specimen under external stimuli.

I. Introduction

The interest in ZnO, a wide-band gap polar semiconductor with large exciton binding energy (60 meV),[1,2] has been renewed by its potential applications in transparent electronics and UV optoelectronic devices operating at room temperature.[3−10] In polar semiconductors, carriers being excited to high energy will relax toward their ground state mainly by Fröhlich interaction with the longitudinal optical phonons.[11] Thus, knowledge of the vibrational properties of this material is of fundamental importance to the understanding of processes such as electron−phonon coupling, phonon−photon interaction, phonon transport, and thermal conductivity, all of which have great impact on optoelectronic device performance. Raman spectroscopy is one of the most powerful tools for investigating the vibronic behavior of atoms due to nondestructive and very sensitive to changes in material properties.[9,10] Recently, Raman vibration of ZnO, under external stimulus such as the change of temperature and pressure, in particular, have been investigated extensively. Generally, all the acoustic and optic modes of ZnO are stiffened under high pressure and softened under high temperature.[11−18]

ZnO with wurtzite structure belongs to the C_{6v}^4 symmetry group. At the Γ point of Brillouin zone, optical phonons have the following irreducible representation: $\Gamma_{opt} = A_1 + 2B_1 + E_1 + 2E_2$, where the A_1 and the E_1 modes are polar and can be split into transverse (TO) and longitudinal optical (LO) phonons, with all being the Raman and infrared active. Nonpolar E_2 modes are the Raman active, while B_1 modes are the Raman inactive.[7,11,17] These Raman modes contain important physical information. For example, E_2 (high) mode represents the bending modes of O−O atoms.[19] In order to verify the proposed approach, we calculated and compared with temperature dependence[20] and pressure dependence[18] of the Raman shift of ZnO crystal. In the past few decades, the availability of bulk ZnO crystals of very high optical quality and the technological relevance of this material have spurred the realization of fundamental and more detailed studies on ZnO lattice dynamics. However, our knowledge of the lattice dynamics of ZnO is still rather limited. In fact, detailed measurements of the optical phonon branch by inelastic neutron scattering are still lacking.

Numerous theoretical models have been developed to interpret the Raman shift induced by thermal stimuli. These models include anharmonic phonon decay,[13] thermal expansion,[15] phonon−phonon interaction,[21] modified phonon decay,[22] and frequency perturbation mechanism.[11,14] Among the models, the perturbation theory has been elegantly accepted, which is described as follows,[11,14]

$$\omega(T) = \omega(0) + \Delta\omega_e(T) + \Delta\omega_d(T)$$

where

$$\Delta\omega_e(T) = -\omega(0)\gamma \int_0^T [\alpha_c(T) + 2\alpha_a(T)]\, dT$$

$$\Delta\omega_d(T) = C\left[1 + \frac{2}{N(\omega,T) - 1}\right] + D\left[1 + \frac{3}{N(\omega,T) - 1} + \frac{3}{\{N(\omega,T) - 1\}^2}\right] + \text{higher order terms}$$

where $\omega(0)$ is the Raman frequency measured at 0 K reference temperature, $\Delta\omega_e(T)$ is the contribution from the thermal expansion; $\Delta\omega_d(T)$ is due to the anharmonic coupling of phonons of other branches. γ is the Gruneisen parameter, C and D are the anharmonic parameters used to fit to the measurement. α_c and α_a are the thermal expansion coefficients along the *a*- and *c*-axis of a wurtzite-type structure. $N(\omega,T)$ is a function of frequency and temperature.

* Corresponding authors. E-mail: ylwxtu@xtu.edu.cn (L.W.Y.); ecqsun@ntu.edu.sg (C.Q.S.).

† Affiliation at Xiangtan University is associated with an honorary appointment.

10.1021/jp909952c
Published on Web 01/07/2010

On the other hand, the Raman shift under applied pressure was usually fitted using the quadratic function:[23]

$$\omega(P) = A\omega(0) + BP + CP^2$$

where P is the pressure, A, B, and C are the adjustable parameters needing clear physical indication, and $\omega(0)$ is the Raman frequency under 0 Pa pressure.

Although the existing models could fit numerically to the measurements, there are too many freely adjustable parameters involved. Especially, the physical mechanism behind is far from clear. The objective of this presentation is to report an analytic model developed from the perspective of local bond average (LBA) approach[24,25] without needing freely adjustable parameters. Besides the quantitative information about the Debye temperature and the cohesive energy per discrete atom of the specimen, the developed approach can provide better understanding of the pressure and temperature effect on the Raman shift of ZnO. Theoretical reproduction of the measurements revealed that the thermally softened Raman modes arise from bond expansion and bond weakening due to vibration and that the pressure-stiffened Raman modes result from bond compression and bond strengthening due to mechanical work hardening.

II. Principle

According to the LBA approach,[25] it is possible to connect the macro properties of a specimen to its bonding parameters (bond nature, bond order, bond length, bond energy) by establishing the functional dependence of the measurable quantities to the bonding identities and the response of these bonding identities to the external stimulus such as coordination environment, temperature, pressure, etc. For instance, coordination number reduction leads to the remaining bonds of the undercoordinated atoms to be shorter and stronger. Increasing the measuring temperature causes bond expansion and bond weakening; increasing pressure have an opposite effect of temperature rise on the length and strength of all the bonds due to the energy storage.[24,26] From these perspectives, we have developed the functional dependence of the Raman shift on the atomic coordination (z), bond length (d), the bond energy (E_b), and the reduced mass (m^*), at 0 K and 0 Pa[26]

$$\omega(0) \propto \frac{z}{d_0}\left[\frac{E_b(0)}{m^*}\right]^{1/2} \tag{1}$$

For a given specimen, the z and the reduced mass do not change. The frequency is only bond length and bond energy dependence. Under the applied temperature and pressure, the change of bond length $d(T,P)$ and the bond energy $E_b(T,P)$ follows the relations

$$\begin{aligned} d(T,P) &= d_0[1 + \int_0^t \alpha_i(t)\,\mathrm{d}T][1 + \int_0^p \beta_T\,\mathrm{d}p] \\ E_b(T,p) &= E_b(0)\left\{1 - \frac{1}{E_b(0)}[\Delta E^p + \int_0^T \eta_1(T)\,\mathrm{d}T]\right\} \end{aligned} \tag{2}$$

where $\alpha_i(t)$ is the thermal expansion coefficient, β_T is the compressibility coefficient at constant temperature. β_T is proportional to the inverse of elastic modulus and satisfies the relation

$$\int_0^P \beta_T\,\mathrm{d}p = -\int_0^P \frac{1}{V}\left(\frac{\partial V}{\partial p}\right)\mathrm{d}p$$

where $\eta_1(T)$ is the specific heat per bond, which follows approximately the specific heat of Debye approach and closes to a constant value of $3R$ (R is the ideal gas constant) at high temperature,[27]

$$\eta(T/\theta_D) = \frac{C_V(T/\theta_D)}{z} = \frac{9R}{z}\left(\frac{T}{\theta_D}\right)\int_0^{\theta_D/T}\frac{x^4\exp(x)}{(e^x-1)^2}\,\mathrm{d}x$$

The integration of $\eta_1(T)$ from 0 K to T ($T \le T_m$) or the conventionally termed specific internal energy per bond, $u(T)$, follows the relation

$$u(T/\theta_D) = \frac{U(T/\theta_D)}{z} = \frac{\int_0^T C_V(T)dT}{z} = \frac{9RT}{z}\left(\frac{T}{\theta_D}\right)^3\int_0^{\theta_D/T}\frac{x^3}{e^x-1}dx$$

where θ_D and C_V are the Debye temperature and specific heat, respectively. $U(T/\theta_D)$ represents the increase in the inner energy of a bond due to the thermally activated vibrations.

The ΔE^p is the distortion energy due to the applied pressure, which is written as[28]

$$\Delta E^p = -\int_{V_0}^{V} p(v)\,\mathrm{d}v = -\int_1^{V/V_0} p(v)\,\mathrm{d}x = [\int_0^P v\,\mathrm{d}p - VP]/V_0 \tag{3}$$

The V and P are correlated with the Birch−Mürnaghan isothermal equation of state[29]

$$P(V) = \frac{3B_0}{2}(\xi^{-7/3} - \xi^{-5/3})\left\{1 + \frac{3}{4}(B'_0 - 4)(\xi^{-2/3} - 1)\right\} \tag{4}$$

where B_0 is the static bulk modulus and B'_0 is the first-order pressure derivative of the B_0; the $\xi = V/V_0$ is the ratio of volume of unit cell addressed after and before being compressed, V_0 is the volume of unit cell at 0 K and 0 Pa, $V_0 \cong 48$ Å^3 for ZnO.[30]

Combining eqs 1−4, we can obtain the analytical form for the temperature and pressure dependent Raman shift:

$$\omega(T,P) \propto \frac{z}{d}\left[\frac{E_b(T,P)}{m^*}\right]^{1/2} \propto \frac{[E_b(T,P)]^{1/2}}{d(T,P)}$$

and hence

$$\frac{\omega(T,P)}{\omega(0,0)} = \frac{\left\{1 - \frac{1}{E_b(0)}[\int_0^T \eta_1(T)\,\mathrm{d}T - \int_{V_0}^V p\,\mathrm{d}v]\right\}^{1/2}}{(1 + \int_0^T \alpha(t)\,\mathrm{d}t)(1 + \int_0^P \beta_T\,\mathrm{d}p)} \tag{5}$$

Figure 1a illustrates the reduced Debye specific heat C_V (in units of gas constant R) and its integration with respect to temperature T (or the termed specific internal energy, $U(T/\theta_D)$). At high T, especially when $T > \theta_D$, the integration of the specific heat or the specific internal energy depends linearly on T. At low temperatures, on the other hand, the integration shows a nonlinear relationship with respect to the temperature in a T^4 form. The range of nonlinearity depends highly on the Debye temperature θ_D, which can be seen from $U(T/\theta_D)$ in Figure 1a.

Figure 1b illustrates the V/V_0-P relation with the scattered data being experimental results for ZnO.[30−32] The integration area (see the inset) is the unit-cell distortion energy being stored in the bonds. Clearly, the energy increases nonlinearly with pressure, which can be ascribed to the fact that the V/V_0 of the unit cell becomes smaller upon the specimen being compressed.

III. Results and Discussion

The well-measured temperature dependence of the E_2(high), E_1(LO), and A_1(LO) modes[11,14] and the pressure-induced E_1(LO), E_1(TO), A_1(LO), and A_1(TO) phonon modes for ZnO at room

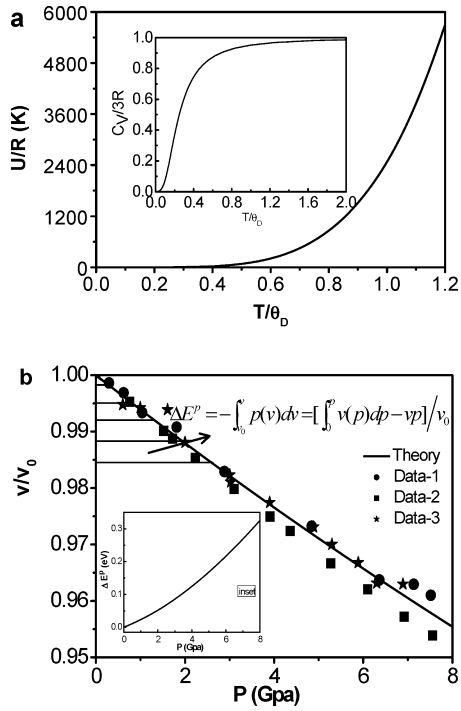

Figure 1. (a) The temperature dependent specific heat (C_V see insert) of ZnO crystals. (b) V/V_0-P relation with the scattered data being experimental results for ZnO.[30−32] The integration area(see the inset) is the unit-cell distortion energy being stored in the bonds.

temperature[17] allows us to verify the presently developed analytical solutions to the temperature and pressure dependence of ZnO Raman shift.

In the numerical calculations, we took the known Debye temperature ($\theta_D = 310$), bulk modulus $B = 160$ GPa, slope $B'_0 = 4.4$,[31] frequency $\omega(0)$,[14,11,17] and the thermal expansion coefficient $\alpha(t)$[33] as input. For ZnO crystal with wurtzite-type structure, the $\alpha(t)$is anisotropic. The principal values of $\alpha(t)$ for these hexagonal structures are those perpendicular and parallel to the c-axis, which are denoted as α_a ($\alpha_a = 6.05 \times 10^{-6} + 2.20 \times 10^{-9}t + 2.29 \times 10^{-14}t^2$) and α_c ($\alpha_c = 3.53 \times 10^{-6} + 2.38 \times 10^{-9}t + 9.24 \times 10^{-14}t^2$),[33] respectively. The effective thermal expansion coefficient $\alpha(t)$is an average of $(2\alpha_a + \alpha_c)/3$.[34] In eq 5, only one fitting parameter of the bond energy $E_b(0)$ is used. Since the thermal expansion coefficient is in a range of 10^{-6} K^{-1}, the term of $1 + \int_0^{T_m}\alpha(t)\,dt \le 1 + 0.012$.[33,35] On the other hand, for $T > \theta_D$, the specific heat (C_V) approaches a constant value and the $U(T/\theta_D)$ is approximately linear dependence on temperature. Hence the relative Raman shift at 0 Pa under the high temperature approximation can be expressed as

$$\frac{\omega(T,0)}{\omega(0,0)} = (1 + \int_0^{T_m}\alpha(t)\,dt)^{-1}\left(1 - \frac{\eta_1 T}{E_b(0)}\right)^{1/2} \approx 1 - \frac{\eta_1 T}{2E_b(0)} \approx 1 - B \times T \quad (6)$$

The experimental slope B_{exp} can be easily determined by fitting to the linear Raman frequency shift versus T curve at high-temperature range. Using the relation of $B_{exp} \cong B = 1/2 \times \eta_1/E_b(0)$ with $\eta_1 \equiv 3R/z$, the mode cohesive energy $E_b(0)$ can be estimated. The derived $E_b(0)$ was then used as an initial input to refine the fitting to the experimental data at the whole temperature range by including the contribution of the nonlinear lattice thermal expansion, which is derived and listed in Table 1.

TABLE 1: Parameters Used in the Matching Theoretical Predictions to the Measured Temperature and Pressure Independence of Raman Shift for ZnO Crystals

Raman mode	ω_0 (cm^{-1})	$E_b(0)$ (eV)
E_2(high)	441.5	1.18
E_1(LO)	595	1.33
E_1(TO)	410	1.32
A_1(LO)	579	1.33
A_1(TO)	378	1.31

Figure 2a shows the theoretical reproduction (solid line) of the measured temperature-dependent Raman shift of E_2(high), E_1(LO), and A_1(LO) modes at atmospheric pressure in all the temperature range.[11,14] At $T \le \theta_D/3$, the relative Raman shift turns from nonlinear to linear when the temperature is increased. The slow decrease of the Raman shift at very low temperatures arises from the small $\int_0^T \eta\,dt$ values as the specific heat $\eta(t)$ is proportional to T^3 at very low temperatures. The results imply that the Debye temperature θ_D determines the width of the shoulder and the $1/E_b(0)$ determines the slopes at high temperature in the curve of temperature dependent Raman shift of ZnO. Figure 2b shows theoretical (solid line) matching of the

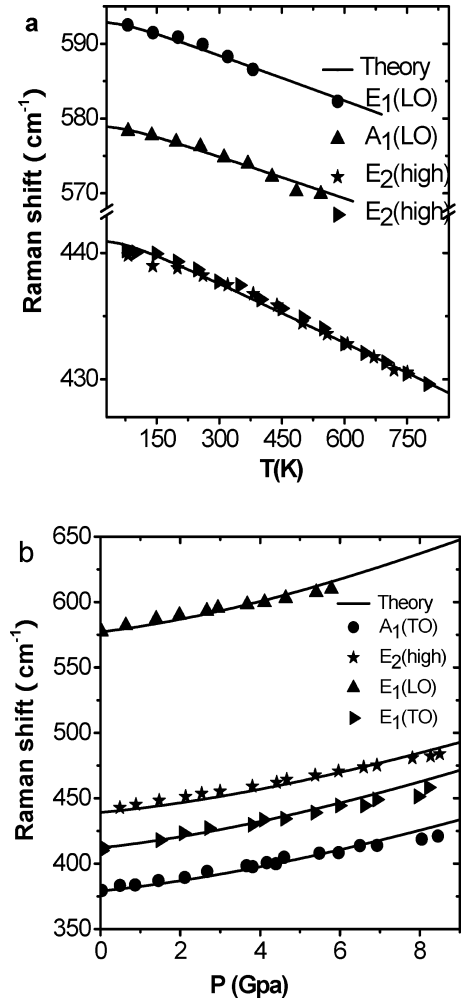

Figure 2. (a) Theoretical (solid) reproduction of the temperature-dependent frequency shift of E_2(high), E_1(LO), and A_1(LO) at a standard atmospheric pressure. The experimental data for E_2(high), E_1(LO), and A_1(LO) are sourced from the refs 11 and 14. (b) Theoretical (solid) reproduction of the measured of the pressure-dependent relation frequency shift of E_1(LO), E_2(high), A_1(TO), and E_1(TO) for ZnO crystals at room temperature, respectively. The experimental data for E_1(LO), E_2(high), A_1(TO), and E_1(TO) are sourced from the ref 17.

measured pressure-dependent Raman shift of E_1(LO), E_1(TO), A_1(LO) and A_1(TO) phonon modes for ZnO at room temperature.[17] The measured blue shift of Raman spectrum under high pressure result from the competition between the thermal expansion the pressure-induced compression.

As demonstrated above, we have been able to reproduce the observations exceedingly well without involving any freely adjustable parameters or employing the mechanisms of phonon decay or the phonon−phonon interaction. Instead, we only consider the length and energy change of a representative bond of the specimen under the applied mechanical stress and temperatures.

On the basis of the BOLS correlation and LBA approach, we disclosed that the optical softening in Si, CdS, InP, TiO_2, CeO_2, and SnO_2 nanocrystals follows eq 1, while the low-frequency acoustic mode hardening is predominated by intergrain interactions.[36] In fact, size-induced acoustic mode hardening was also observed in ZnO nanocrystals below 10 nm.[9,10] Further investigation is in progress on the joint effect of size, shape, temperature, and pressure on the Raman shift of ZnO and other compound materials.

IV. Conclusion

We have presented an analytical expression connecting the macroscopically measurable Raman modes directly to the bonding identities of the specimen and the response of the bonding identities to the applied stimulus for deeper insight into the atomistic origin of the temperature- and pressure-induced Raman shift in ZnO crystals. Theoretical reproduction of the measurements revealed that the thermally softened Raman modes arise from bond expansion and bond weakening due to vibration and that the pressure-stiffened Raman modes result from bond compression and bond strengthening due the mechanical work hardening and energy storing. The presented approach from the perspective of BOLS and LBA would provide a useful yet simple way complementing the investigation of lattice dynamics of ZnO under the stimuli change of atomic coordination, thermal and mechanical activation.

Acknowledgment. The project was supported by Grants from National Natural Science Foundation of China (No.10772157 and No.10802071), Hunan Province, China.

References and Notes

(1) Chen, Y. F.; Tuan, N. T.; Segawa, Y.; Ko, H.-j.; Hong, S.-k.; Yao, T. *Appl. Phys. Lett.* **2001**, *78*, 1469.
(2) Ranjani Viswanatha, S. S.; Satpati, B.; Satyam, P. V.; Dev, B. N.; Sarma., D. D. *J. Mater. Chem.* **2004**, *14*, 661.
(3) Cao, B.; Cai, W.; Zeng, H. *Appl. Phys. Lett.* **2006**, *88*, 161101.
(4) Huang, M. H.; Mao, S.; Feick, H.; Yan, H.; Wu, Y.; Kind, H.; Weber, E.; Russo, R.; Yang, P. *Science* **2001**, *292*, 1897.
(5) Zhao, L.; Lian, J.; Liu, Y.; Jiang, Q. *Appl. Surf. Sci.* **2006**, *252*, 8451.
(6) Yang, L. W.; Wu, X. L.; Huang, G. S.; Qiu, T.; Yang, Y. M. *J. Appl. Phys.* **2005**, *97*, 014308.
(7) Lin, K.-F.; Cheng, H.-M.; Hsu, H.-C.; Lin, L.-J.; Hsieh, W.-F. *Chem. Phys. Lett.* **2005**, *409*, 208.
(8) Wang, Z. L.; Song, J. *Science* **2006**, *312*, 242.
(9) Yadav, H. K.; Gupata, V.; Sreenivas, K.; Singh, S. P.; Sundarakannan, B.; Katiyar, R. S. *Phys. Rev. Lett.* **2006**, *97*, 058802.
(10) Chassaing, P. M.; Demangeot, F.; Combe, N.; Saint-Macary, L.; Kahn, M. L.; Chaudret, B. *Phys. Rev. B (Condens. Matter Mater. Phys.)* **2009**, *79*, 155314.
(11) Cusco, R.; Alarcon-Llado, E.; Ibanez, J.; Artus, L.; Jimenez, J.; Wang, B.; Callahan, M. J. *Phys. Rev. B (Condens. Matter Mater. Phys.)* **2007**, *75*, 165202.
(12) Serrano, J.; Manjon, F. J.; Romero, A. H.; Widulle, F.; Lauck, R.; Cardona, M. *Phys. Rev. Lett.* **2003**, *90*, 055510.
(13) Aku-Leh, C.; Zhao, J.; Merlin, R.; Menendez, J.; Cardona, M. *Phys. Rev. B* **2005**, *71*, 205211.
(14) Samanta, K.; Bhattacharya, P.; Katiyar, R. S. *Phys. Rev. B (Condens. Matter Mater. Phys.)* **2007**, *75*, 035208.
(15) Serrano, J.; Romero, A. H.; Manjon, F. J.; Lauck, R.; Cardona, M.; Rubio, A. *Phys. Rev. B* **2004**, *69*, 094306.
(16) Mitra, S. S.; Brafman, O.; Daniels, W. B.; Crawford, R. K. *Phys. Rev.* **1969**, *186*, 942.
(17) Decremps, F.; Pellicer-Porres, J.; Saitta, A. M.; Chervin, J.-C.; Polian, A. *Phys. Rev. B* **2002**, *65*, 092101.
(18) Mead, D. G.; Wilkinson, G. R. *J. Raman Spectrosc.* **1977**, *6*, 123.
(19) Cardona, M. T., M. L. W. *Rev. Mod. Phys.* **2005**, *77*, 1173.
(20) Damen, T. C.; Porto, S. P. S.; Tell, B. *Phys. Rev.* **1966**, *142*, 570.
(21) Cui, J. B.; Amtmann, K.; Ristein, J.; Ley, L. *J. Appl. Phys.* **1998**, *83*, 7929.
(22) Menéndez, J.; Cardona, M. *Phys. Rev. B* **1984**, *29*, 2051.
(23) Liu, J.; Vohra, Y. K. *Phys. Rev. Lett.* **1994**, *72*, 4105.
(24) Ouyang, G.; Sun, C. Q.; Zhu, W. G. *J. Phys. Chem. C* **2009**, *113*, 9516.
(25) Sun, C. Q. *Prog. Mater. Sci.* **2009**, *54*, 179.
(26) Gu, M. X.; Pan, L. K.; Tay, B. K.; Sun, C. Q. *J. Raman Spectrosc.* **2007**, *38*, 780.
(27) Álvarez-Ramírez, J.; Valdés-Parada, F. J.; Ochoa-Tapia, J. A. *Phys. Lett. A* **2005**, *345*, 231.
(28) Chen, Z.; Sun, C. Q.; Zhou, Y.; Ouyang, G. *J. Phys. Chem. C* **2008**, *112*, 2423.
(29) He, Y.; Liu, J. F.; Chen, W.; Wang, Y.; Wang, H.; Zeng, Y. W.; Zhang, G. Q.; Wang, L. N.; Liu, J.; Hu, T. D.; Hahn, H.; Gleiter, H.; Jiang, J. Z. *Phys. Rev. B* **2005**, *72*, 212102.
(30) Sowa, H. *J. Appl. Crystallogr.* **2006**, *39*, 169.
(31) Karzel, H.; Potzel, W.; Koferlein, M.; Schiessl, W.; Steiner, M.; Hiller, U.; Kalvius, G. M.; Mitchell, D. W.; Das, T. P.; Blaha, P.; Schwarz, K.; Pasternak, M. P. *Phys. Rev. B* **1996**, *53*, 11425.
(32) Decremps, F.; Datchi, F.; Saitta, A. M.; Polian, A.; Pascarelli, S.; Di Cicco, A.; Iti, J. P.; Baudelet, F. *Phys. Rev. B* **2003**, *68*, 104101.
(33) Khan, A. A. *Acta Crystallogr., Sect. A* **1968**, *24*, 403.
(34) Slack, G. A.; Bartram, S. F. *J. Appl. Phys.* **1975**, *46*, 89.
(35) Yang, C.-J.; Wang, S.-M.; Liang, S.-W.; Chang, Y.-H.; Chen, C.; Shieh, J.-M. *Appl. Phys. Lett.* **2007**, *90*, 033104.
(36) Sun, C. Q.; Pan, L. K.; Li, C. M.; Li, S. *Phys. Rev.* **2005**, *72*, 134301.

JP909952C